# Brillouin Optical Time-Domain Analyzer Assisted by Support Vector Machine for Ultrafast Temperature Extraction

Huan Wu, Liang Wang, *Member, OSA*, Nan Guo, Chester Shu, *Senior Member, IEEE*, and Chao Lu, *Fellow, OSA*

***Abstract*—Brillouin optical time-domain analyzer (BOTDA) assisted by support vector machine (SVM) for ultrafast temperature extraction is proposed and experimentally demonstrated. The temperature extraction is treated as a supervised classification problem and the Brillouin gain spectrum (BGS) is classified into each temperature class according to the support vectors and hyperplane of the SVM model after training. Ideal pseudo-Voigt curve-based BGS is used to train the SVM to get the support vectors and hyperplane. The performance of SVM is investigated in both simulation and experiment under various conditions for BGS collection. Both simulation and experiment results show that SVM is more robust to a wide range of signal-to-noise ratios, averaging times, pump pulse widths, frequency scanning steps, and temperatures. In addition to better accuracy, the processing speed for temperature extraction using SVM is 100 times faster than that using conventional Lorentzian curve and pseudo-Voigt curve fitting techniques in our experiment. The fast processing speed together with good accuracy and robustness makes SVM a highly competitive candidate for future high-speed BOTDA sensors**

***Index Terms*—Brillouin optical time domain analyzer, fiber optics sensors, stimulated Brillouin scattering, support vector machine.**

## I. Introduction

STIMULATED Brillouin scattering (SBS) in optical fibers is a stimulated inelastic scattering which involves the interaction between optical photons and acoustic phonons and gives rise to a backscattered Stokes light with optical frequency downshifted by a Brillouin frequency shift (BFS) [1]. Strain and temperature changes in the optical fiber induce variations on the acoustic velocity and refractive index, resulting in temperature and strain dependence of the BFS [2]. Sensor systems based on SBS have been developed for temperature and strain monitoring, of which the configuration of Brillouin optical time domain analyzer (BOTDA) has attracted intensive research interest due to its capability in distributed and precise measurement of strain and temperature profile along fibers [3]–[9]. To extract temperature and strain information in a BOTDA system, the BFSs need to be determined from the measured Brillouin gain spectra (BGSs), where curve fitting methods are commonly used and the BFS of the measured BGS is taken as the frequency of the peak gain on fitted curves [10]–[17]. As the actual BGS obtained from BOTDA measurement is the convolution between the pump pulse spectrum and the intrinsic Lorentzian gain spectrum, its profile can be fitted using Lorentzian curve [10]–[12] or Gaussian curve [13]. Depending on the pump pulse duration, the actual BGS practically has a line shape in between Lorentzian curve and Gaussian curve which is more like a Voigt curve and can be well approximated by the pseudo-Voigt curve [14]–[16]. Least square-error fitting based on Levenberg- Marquardt algorithm (LMA) has been widely used in Lorentzian curve and pseudo-Voigt curve fitting [16]. Another type of curve fitting method is the quadratic curve fitting which assumes the actual BGS has a quadratic lineshape near its peak area [17]. However, most of the curve fitting techniques require the initialization of model parameters and poor initialization will result in significant degradation of the accuracy in BFS determination [12], [18], [19]. In addition, the performance of curve fitting techniques will also degrade quickly if there are only fewer data points collected on the measured BGS, i.e., adopting large frequency scanning step during the acquisition of the BGSs [17]. Moreover, due to the iterative feature, the curve fitting techniques usually require long processing time to extract BFS from the measured BGS, especially when a large number of BGSs are collected and processed along a long sensing fiber.

In addition to curve fitting techniques, a non-curve-fitting technique called cross-correlation method (XCM) is also proposed based on calculation of cross-correlation between an ideal Lorentzian curve and the measured BGS to determine the BFS [18], [19]. Unlike curve fitting techniques, XCM does not suffer from the problem of initial parameter setting, but it requires data interpolation process to up-sample the measured BGS for good accuracy which in turn increases the data processing time and hence results in a tradeoff between the accuracy and processing speed. Recently Artificial Neural Network (ANN) has been successfully used in a BOTDA system to directly extract temperature distribution from the measured BGSs along the sensing fiber [20]. Nevertheless, ANN requires lots of

Manuscript received May 6, 2017; revised July 8, 2017; accepted August 8, 2017. Date of publication August 13, 2017; date of current version September 5, 2017. This work was supported in part by the Research Grants Council of Hong Kong Project: CUHK GRF 416213, 14206614, 14238816, and PolyU 5208/13E; and in part by the National Natural Science Foundation of China: NSFC 61377093, 61435006. *(Corresponding author: Liang Wang.)*

H. Wu, L. Wang, and C. Shu are with the Department of Electronic Engineering, Chinese University of Hong Kong, Sha Tin, Hong Kong (e-mail: hwu@ee.cuhk.edu.hk; lwang@ee.cuhk.edu.hk; ctshu@ee.cuhk.edu.hk).

N. Guo and C. Lu are with the Department of Electronic and Information Engineering, Hong Kong Polytechnic University, Kowloon, Hong Kong (e-mail: neil.nan.guo@outlook.com; enluchao@polyu.edu.hk).

Color versions of one or more of the figures in this paper are available online at http://ieeexplore.ieee.org.

Digital Object Identifier 10.1109/JLT.2017.2739421

empirical trials in the training phase to find a suitable architecture, e.g., the number of layers, number of neurons in each layer and connecting weights among neurons, which usually takes at least several hours and is thus very time-consuming. Even with numerous trials, best results still cannot be guaranteed as backpropagation algorithm for ANN training usually converges only to locally optimal solutions [20]. Moreover, in Ref. [20] since only particular experiment parameters are used for BGS collection, i.e., 40 ns pump pulse and 2000 averaging times, the tolerance of data processing method to different pump pulse widths, averaging times and signal-to-noise ratio (SNR) are not investigated.

On the other hand, Support Vector Machine (SVM) is a popular kind of signal processing models to analyze data for classification and regression. Based on the statistical learning theory, SVM has gained lots of attention due to both theoretical and computational merits [21], [22] and has been well applied to many fields such as hand-written character recognition [23], cancer classification [24], remote sensing [25] and mitigation of fiber nonlinearity in optical communications [26]. Compared with ANN, SVM has a strong founding theory without the time-consuming training and requires less memory to store the predictive model. More importantly, SVM can always guarantee a globally optimal solution as it is a convex optimization problem. In this paper, we propose a BOTDA system assisted by SVM for fast processing of the measured BGSs to extract temperature information. The temperature extraction is treated as a supervised classification problem and the BGSs are classified into each temperature class by SVM. The paper is organized as follows. Section II describes the principle of using SVM for temperature extraction and how to train the SVM model. Simulation are conducted in this section to investigate the performance of SVM compared with that of conventional Lorentzian curve fitting (LCF) and pseudo-Voigt curve fitting (pVCF) techniques. In Section III, we experimentally analyze the temperature extraction using SVM under various conditions of BGS collection, i.e., different averaging times or signal-to-noise ratios (SNRs), pump pulse widths, frequency scanning steps, and verify the simulation results in Section II. The processing speed of SVM is discussed and compared with conventional curve fitting techniques in this section. The study is concluded in Section IV.

## II. Principle and Simulation

### A. Principle of Using SVM for Temperature Extraction and SVM Training

SVM is a discriminative classifier determining boundaries to distinguish different classes of data. Fig. 1 illustrates a simple scenario of two-class separable classification problem using SVM. The data samples for the two classes (red and blue class) are represented by a feature vector $\mathbf{X} = (x_1, x_2)$ where two dimensional feature space is assumed for simplicity. The strategy of SVM is to find a maximum-margin hyperplane together with support vectors (data samples closest to the hyperplane) to separate and classify the input feature vectors from the two different classes. The hyperplane can be expressed as:

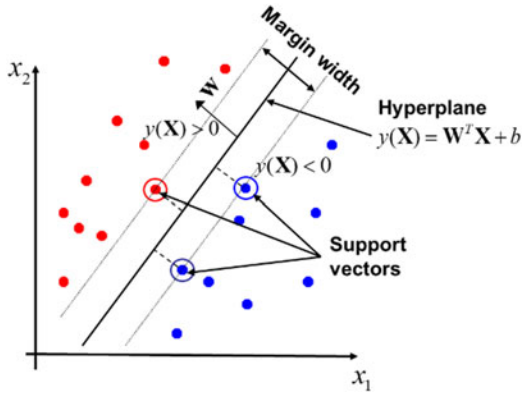


Fig. 1. Illustration of a two-class separable classification problem in a two-dimensional feature space using SVM.

$$y(\mathbf{X}) = \mathbf{W}^{\mathrm{T}}\mathbf{X} + b \tag{1}$$

where $\mathbf{W}$ is the norm vector of the hyperplane and b is intercept. The hyperplane and support vectors are learned from training samples and hence the values of $\mathbf{W}$ and b are determined to maximize the margin width during the training phase of SVM. The training samples can be expressed as $S = \{(\mathbf{X}_i, l_i), i = 1, \cdots, N\}$, where N is the number of training samples and the label $l_i = \pm 1$ indicating which class $\mathbf{X}_i$ belongs to, e.g., $l_i = -1$ if $y(\mathbf{X}_i) < 0$ when $\mathbf{X}_i$ belongs to the blue class in Fig. 1. The training of SVM is an optimization problem which can be solved using quadratic programming (QP) method [27], [28]. In QP method, the norm vector $\mathbf{W}$ is a linear combination of the training feature vectors $\mathbf{X}_i$:

$$\mathbf{W} = \sum_{i=1}^{N} \alpha_i l_i \mathbf{X}_i \tag{2}$$

where $\alpha_i$ is the Lagrange multiplier introduced in the optimization process, and has non-zero values only for support vectors. After training by QP method, the SVM model with optimal hyperplane and support vectors is ready for classification purpose. In the testing phase, the inner product between support vectors and input feature vectors are calculated to obtain $y(\mathbf{X}_t)$,

$$y(\mathbf{X}_t) = \mathbf{W}^T\mathbf{X}_t + b = \sum \alpha_i l_i (\mathbf{X}_s \cdot \mathbf{X}_t) + b \tag{3}$$

where $\mathbf{X}_s$ and $\mathbf{X}_t$ represent support vectors and test vectors, respectively. Then the type of class that $\mathbf{X}_t$ belongs to is determined by the sign of $y(\mathbf{X}_t)$. In practical situation, many problems involve identification of multiple classes with high-dimensional vector $\mathbf{X} = (x_1, \ldots, x_n)$ and simple SVM classifier is operated as multi-class classifier by using method such as 'one-against-one' [29]. This method constructs one binary classifier for each pair of classes, thus for a problem with $k$ classes, $k(k-1)/2$ binary classifiers are constructed and trained to distinguish the samples of one class from another class. After all binary classifiers are constructed in the training phase, classification of an unknown test sample is done according to maximum voting. During maximum voting the unknown test sample is classified into one of the two classes by each binary classifier

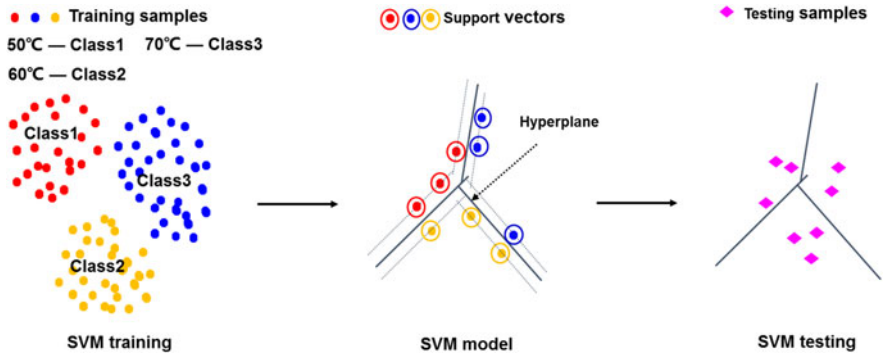


Fig. 2. Principle of using SVM to extract temperature information from BGSs.

and obtains one vote for this class, and then after the classification by all the binary classifiers the class receiving the most votes is selected as the class which the unknown test sample belongs to.

In our case, a linear multi-class SVM classifier is used to extract temperature information from the BGSs measured by BOTDA, since multiple temperature classes with each temperature value forming one class are required for this purpose. The principle is illustrated in Fig. 2. Each data sample either for training or testing, i.e., a red or yellow or blue or pink dot in Fig. 2, indicates a BGS which has many data points on it. The data points on the BGS consists of the feature vector space for that data sample and the number of the data points determines the dimension of the vector space. Thus the vector space in our case is a multiple dimension space. In Fig. 2 we use 50 °C, 60 °C, 70 °C as example to form three temperature classes (Class1, Class2 and Class 3). The training samples (i.e., BGSs) represented by red dots belong to Class1, which means those BGSs are for the temperature of 50 °C. Similarly, the training BGSs represented by yellow dots and blue dots belong to Class2 (60 °C) and Class3 (70 °C), respectively. In the training phase, the known BGSs together with the corresponding labels serve as the training samples to determine the high-dimensional hyperplane and support vectors of the SVM model for temperature extraction. While in the testing phase each measured BGS as the testing sample is classified into one class of temperatures, i.e., Class1, Class2 and Class 3, by the SVM model and the corresponding temperature value is taken as the measured temperature.

For SVM training, we use pseudo-Voigt curve as the gain profile of ideal BGSs. Pseudo-Voigt curve is selected to make one single SVM model suitable for conditions of all different pump pulse widths. The pseudo-Voigt curve is a combination of Lorentzian and Gaussian curves [16]:

$$f(\upsilon) = g_B \left\{ c \frac{1}{1 + [(\upsilon - \upsilon_B)/(\Delta\upsilon_B/2)]^2} + (1-c)\exp\left[ -\ln 2 \left( \frac{\upsilon - \upsilon_B}{\Delta\upsilon_B/2} \right)^2 \right] \right\} \quad (4)$$

where $g_B$ is the peak gain, $\upsilon_B$ is the BFS, $\Delta\upsilon_B$ is the linewidth and $c$ is the proportion taken by Lorentzian component. The BFSs of the ideal BGSs from a temperature range of 20 °C to 70 °C are determined using a temperature coefficient of 0.9856 MHz/ °C which is calibrated for our fiber under test (FUT). Here we use three different temperature steps (1 °C, 0.5 °C and 0.1 °C) to form the temperature classes respectively (1 °C, 0.5 °C and 0.1 °C steps corresponds to 51 classes, 101 classes, and 501 classes, respectively), and hence three corresponding SVM models, i.e., SVM-1 °C, SVM-0.5 °C and SVM-0.1 °C, are separately trained to extract the temperature. For each temperature class, we obtain the ideal BGSs with the same BFS but with different linewidth varying from 30 MHz to 100 MHz at a step of 2 MHz in order to accommodate BGS linewidth variations. At the same time the lineshape factor $c$ in (4) varies to traverse all the values from 0 to 1 at a step of 0.2 which also accounts for different pump pulse widths. Finally we have 51 × 36 × 6, 101 × 36 × 6, and 501 × 36 × 6 training samples to train the SVM-1 °C, SVM-0.5 °C and SVM-0.1 °C, respectively. The frequency range of $\upsilon$ in (4) is from 10.791 GHz to 10.99 GHz, the same as the frequency scanning range during the acquisition of BGSs. As an example, if $\upsilon$ takes 1 MHz step, there are 200 data points on each BGS serving as its feature vector space, i.e., feature $x_1$ to $x_{200}$, and thus the dimension of the vector space is 200.

### *B. LMA Based LCF and pVCF for BFS Extraction*

In this part, Levenberg-Marquardt algorithm (LMA) we adopt in LCF and pVCF for BFS extraction is described. LMA is a kind of iterative algorithm to solve local minimum problem of nonlinear multivariate real functions, and it is a combination of the gradient descent method and Gauss-Newton method [12], [16], [19]. The model for LCF and pVCF can be expressed in terms of a vector $\vec{p}$ as follows:

$$g(\upsilon_i, \vec{p}) = \frac{p_1}{1 + 4\left(\frac{\upsilon_i - p_2}{p_3}\right)^2} \quad (5)$$

$$g(\upsilon_i, \vec{p}) = p_1 \left\{ p_4 \frac{1}{1 + 4\left(\frac{\upsilon_i - p_2}{p_3}\right)^2} + (1-p_4)\exp\left[ -In2\left( 4\left( \frac{\upsilon_i - p_2}{p_3} \right)^2 \right) \right] \right\} \quad (6)$$

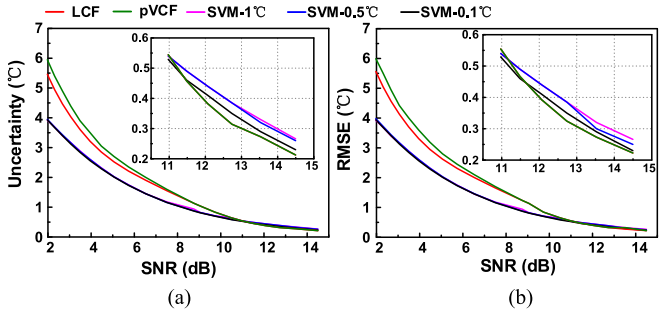


Fig. 3. (a) Temperature uncertainty, (b) root mean square error (RMSE) simulated under different SNRs. Insets: zoom-in view of (a) and (b) for SNR from 11 to 14.5 dB. The temperature to be measured is set at 50 °C.

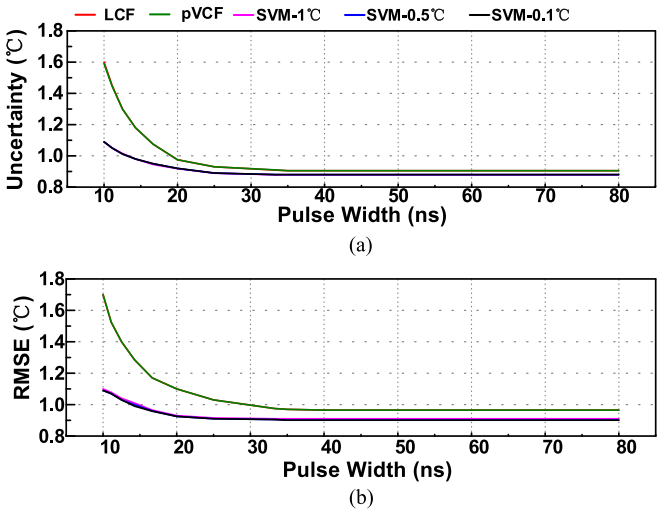


Fig. 4. (a) Temperature uncertainty, (b) RMSE simulated under different under different pump pulse widths. The temperature to be measured is set at 50 °C.

where $\vec{p} = (p_1, p_2, p_3)$ for LCF and $\vec{p} = (p_1, p_2, p_3, p_4)$ for pVCF. In vector $\vec{p}$, $p_1$ is the gain parameter, $p_2$ is the central frequency parameter, $p_3$ is the linewidth parameter, and $p_4$ is the shape coefficient. In both (5) and (6) $\upsilon_i$ represents the $i$th scanned frequency. The curve fitting process starts with an initial guess for the vector $\vec{p}$, and then $\vec{p}$ is iteratively updated until squared error $\chi^2$ converges, where $\chi^2$ is expressed as:

$$\chi^2 = \sum^{N} \left[ \frac{(g - g(\upsilon_i, \vec{p})}{\sigma_i} \right]^2 \tag{7}$$

with N as the number of scanned frequencies, and $\sigma_i$ as the standard deviation of the noise. The initial values of $p_1$, $p_2$, $p_3$ and $p_4$ are set to be the maximum value of the measured g, the frequency at the maximum value of g, 50 MHz and 1, respectively.

### C. Simulation Results

Before using SVM to extract temperature information from the measured BGSs, we first evaluate its performance by using simulated BGSs in the testing phase. In the simulation, the BFSs of the simulated BGSs is determined using the temperature coefficient of the FUT in the experiment. Then by adding Gaussian white noise to ideal Lorentzian curve, we obtain noisy Lorentzian curves as the simulated BGSs. At first the linewidth of the simulated BGSs is fixed at $\Delta\upsilon_B = 50$ MHz, to simulate the condition for a pump pulse width around 20 ns. The step of frequency $\upsilon$ is fixed at 1 MHz, corresponding to a frequency scanning step of 1 MHz. The SNR of the simulated BGSs is controlled by adding Gaussian white noise. Then three SVM models (SVM-1 °C, SVM-0.5 °C and SVM-0.1 °C) after training are employed to extract temperature from the simulated BGSs. The simulation is run 1000 times to make the results reliable for statistical analysis. Fig. 3 shows the temperature uncertainty and root mean square error (RMSE) simulated under different SNRs by using SVMs for temperature extraction. The temperature uncertainty is defined as the standard deviation of the extracted temperature and the RMSE is calculated using the temperatures measured by the thermometer and extracted by SVM or curve fitting techniques. Here the SNR is defined as the ratio between the mean amplitude of Brillouin peak or trace and its standard deviation [30], [31], which is proportional to the amplitude instead of power. The temperature to be measured is set at 50 °C. The performance of SVM-1 °C, SVM-0.5 °C and SVM-0.1 °C are almost the same, but SVM-0.1 °C is slightly better than SVM-1 °C and SVM-0.5 °C when the SNR is beyond 11 dB. For comparison, we also gives the results by using LCF and pVCF to determine the BFS and then covert from BFS to temperature. From the results we can see that both of the uncertainty and RMSE by using SVMs and curve fitting methods (i.e., LCF and pVCF) decrease as the SNR increases. At SNR beyond 12 dB, the performance of curve fitting methods is slightly better than SVMs but they are still at comparable level; while as the SNR is reduced, the uncertainty and RMSE using SVMs become smaller than those using LCF and pVCF, which implies that at low SNR SVMs have better accuracy than LCF and pVCF.

Next we change the pump pulse width to investigate the tolerance of SVMs to different pump pulse widths. The SNR of the simulated BGSs is now fixed at 9 dB and the pump pulse width varies from 10 ns to 80 ns. The results are plotted in Fig. 4. Like those in Fig. 3, all three SVM models (SVM-1 °C, SVM-0.5 °C and SVM-0.1 °C) have similar performance. Both of the uncertainty and RMSE by using SVMs and curve fitting methods (i.e., LCF and pVCF) increases as the pump pulse width decreases due to large linewidth at narrow pump pulse width. However, the degradation of uncertainty and RMSE using SVMs is much smaller than that using curve fitting methods, which implies that SVMs have better tolerance to the variation of pump pulse width than curve fitting methods. LCF and pVCF start with initial values, then fitting algorithm iteratively update the parameters until it converges to local minima dependent on initial values. For this reason, the initialization of the fitting parameters with values close to the expected ones becomes important to have accurate fitting results. Thus LCF and pVCF have worse tolerance to the change of pump pulse width compared with SVMs which are trained by training samples with various linewidth and shape factor $c$ considered. Note that in

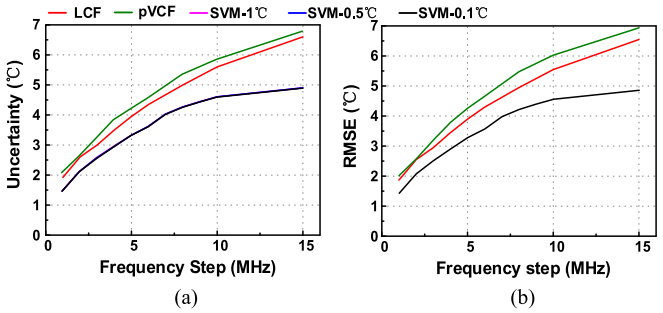


Fig. 5. (a) Temperature uncertainty, (b) RMSE simulated under different frequency scanning steps. The temperature to be measured is set at 50 °C.

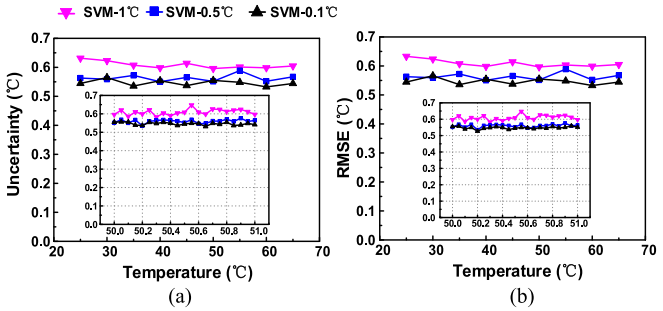


Fig. 6. (a) Temperature uncertainty, (b) RMSE simulated for temperature range from 25 °C to 65 °C at a step of 5 °C. Insets: results for small temperature range from 50 °C to 51 °C at a step of 0.05 °C.

Fig. 4 when the pulse width is beyond 40 ns, the uncertainty and RMSE only have little change due to the same fixed SNR for different pulse widths and also the fact that the BGS linewidth approaches the intrinsic SBS linewidth (30 MHz in our case) at large pulse width.

The step of frequency $\upsilon$ determines the number of features in each feature vector, i.e., number of data points on each BGS. Here we also change the step of $\upsilon$ to study the SVM performance under different frequency scanning steps. The linewidth of the simulated BGSs is fixed at 50 MHz and the SNR is now set at a relatively low value of 6.5 dB. The results are given in Fig. 5. Again all three SVM models give almost the same performance. As the frequency step increases, there are fewer data points on each simulated BGS, leading to worse uncertainty and RMSE for both SVMs and curve fitting methods (i.e., LCF and pVCF). At each frequency step, both temperature uncertainty and RMSE using SVMs are lower than that using LCF and pVCF, and the performance degradation of SVMs is more slowly at large scanning step, which implies that the SVMs can tolerate a wider range of frequency steps compared with LCF and pVCF. Note that LCF shows a little better performance than pVCF because our simulated BGSs is generated from ideal Lorentzian curve with Gaussian white noise added.

To examine the performance of SVM in a wider temperature range, we change the temperature from 25 °C to 65 °C at a step of 5 °C while fix the linewidth of the simulated BGSs at 50 MHz and SNR at 11 dB. The temperature is extracted by using SVM-1 °C, SVM-0.5 °C and SVM-0.1 °C, respectively and the results are given in Fig. 6. Insets of Fig. 6 also show the results in a small

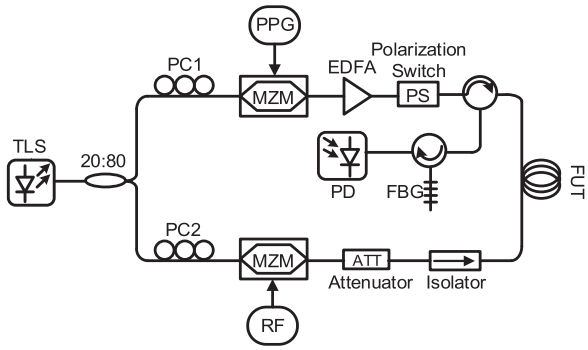


Fig. 7. BOTDA experiment setup. TLS: tunable laser source, PC: polarization controller, PPG: pulse pattern generator, RF: radio frequency, PS: polarization switch, MZM: Mach-Zehnder modulator, FUT: fiber under test, FBG: fiber-Bragg grating, PD: photodetector.

temperature range from 50 °C to 51 °C at a step of 0.05 °C. The uncertainty and RMSE using SVM-1 °C is a little worse than those using SVM-0.5 °C and SVM-0.1 °C (maximum difference is around 0.1 °C) because it has a littler larger temperature step to form temperature class. The maximum fluctuation of the uncertainty and RMSE are 0.065 °C and 0.062 °C for SVM-1 °C, 0.038 °C and 0.042 °C for SVM-0.5 °C, 0.032 °C and 0.034 °C for SVM-0.1 °C, respectively. From the results we can see that SVM-1 °C, SVM-0.5 °C and SVM-0.1 °C almost have comparable performance under different temperatures.

Since all three SVM models (SVM-1 °C, SVM-0.5 °C and SVM-0.1 °C) have similar performance, we only use SVM-0.5 °C in the following section to demonstrate the extraction of temperature from the measured BGSs.

## III. BOTDA Setup and Experiment Results

The BOTDA experiment setup is shown in Fig. 7. The output of a tunable laser is set at 1550 nm and is split into two branches using a 20/80 coupler. The CW light in the upper branch is modulated by a Mach-Zehnder modulator (MZM) with extinction ratio of 40 dB to generate optical pump pulses. The pump is then amplified by an erbium-doped fiber amplifier (EDFA) and passes through a polarization switch (PS) which is used to obtain Brillouin traces from orthogonal pump pulses to suppress polarization dependent noise. In the lower branch, another high-extinction ratio MZM, driven by a microwave signal generator and biased at Null point, is used to generate a carrier suppressed double-sideband probe signal. An optical attenuator is used to control the probe power followed by an isolator to block the signal from the pump branch. The probe is delivered into the FUT where it is amplified by the counter-propagating pump. Finally, the probe signal is detected by a 125-MHz photodetector after the lower-frequency probe sideband is selected by using a fiber Bragg grating (FBG) filter. Brillouin time domain traces after averaging are collected using an oscilloscope at a sampling rate of 250 MSample/s and the local BGSs are reconstructed with microwave frequency scanned from 10.791 GHz to 10.99 GHz. To completely evaluate the performance of SVM under different experiment conditions, different pump pulse widths, averaging

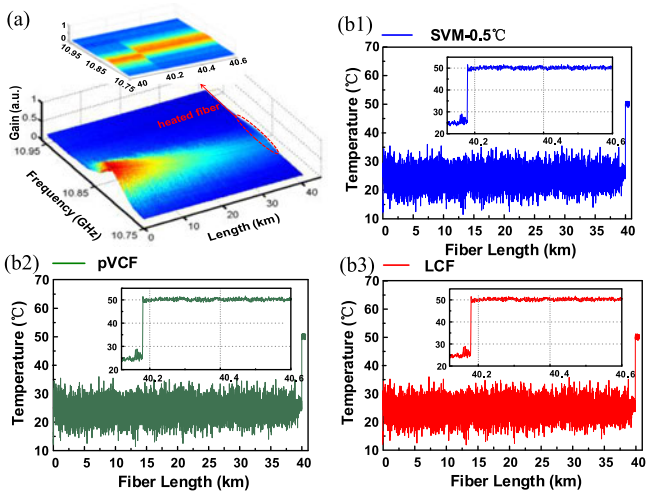


Fig. 8. (a) Measured BGS distribution along 40.6 km FUT with last 400 m section heated at 50 °C; inset: zoom-in view at the heated section. (b1)–(b3) Temperature distribution along FUT extracted by SVM-0.5 °C, LCF, and pVCF; insets: zoom-in view at the heated section. 20 ns pump pulse, 1000 times averaging and 1 MHz frequency scanning step are used for the measurement.

times, and frequency scanning steps are employed in the experiment to measure the BGSs for processing.

The FUT is a 40.6 km long single-mode fiber and last 400 m section, corresponding to 1000 sampling points, is free from strain and put into the oven. Long fiber section is heated in order to provide sufficient data points for analysis of statistical performance of SVM. Fig. 8(a) shows the BGSs distribution measured with 20 ns pump pulse, 1000 times averaging and 1 MHz frequency scanning step. The measured BGSs are processed by the same SVM-0.5 °C as in Section II and the temperature along FUT is directly extracted and given as the blue curve in Fig. 8(b1). In comparison, we also plot the temperature distribution calculated from BFS distribution using LCF and pVCF, as shown by the red and green curves in Fig. 8(b2) and (b3). The insets in Fig. 8 depict the zoom-in view at the heated section. We can see that the temperature information along FUT has been successfully extracted by SVM-0.5 °C without the need of determination of BFS, and conversion from BFS to temperature. The temperature uncertainty and RMSE at the last 400 m FUT are calculated to be 0.4655 °C and 0.501 °C for SVM-0.5 °C, 0.4587 °C and 0.5505 °C for LCF, 0.4589 °C and 0.551 °C for pVCF, respectively. With 1000 averaging times the SNR is relatively high (∼11.5 dB) such that the performance of both SVM-0.5 °C and curve fitting methods are at comparable level, which agrees well with our simulation results. Note that the noisy temperature distribution before the heated section is due to the uneven strain distribution along the section wound on the fiber reel, which affects the accuracy of the temperature measurement.

Then we investigate the tolerance of SVM to different SNRs. Using 20 ns pump pulse and 1 MHz frequency scanning step we collect the BGSs under different trace averaging times (i.e., 8, 16, 50, 200, 400, 1000). And the measured SNRs are calculated to be 2.9 dB, 4.3 dB, 6.1 dB, 8.6 dB, 9.9 dB, 11.5 dB,

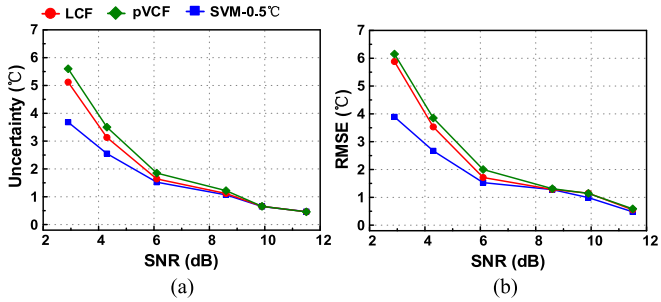


Fig. 9. (a) Temperature uncertainty, (b) RMSE measured around the last 400 m section by using SVM-0.5 °C, LCF and pVCF for temperature extraction, respectively. 20 ns pump pulse and 1 MHz frequency scanning step are used for the measurement under different SNRs. The temperature in the oven is set to be 50 °C.

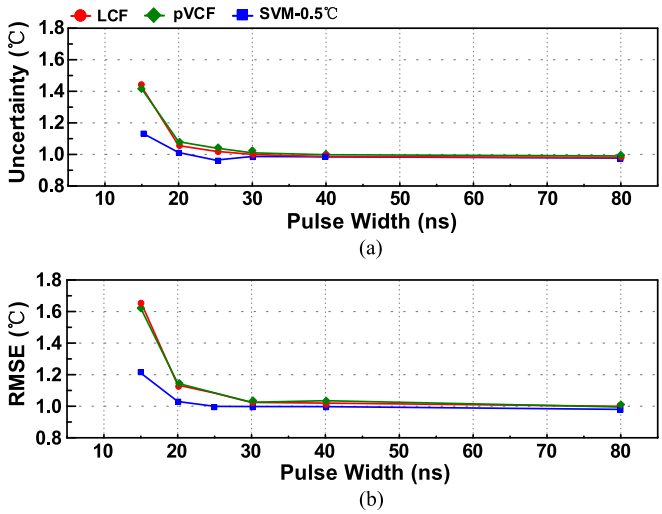


Fig. 10. (a) Temperature uncertainty, (b) RMSE measured by using SVM-0.5 °C , LCF and pVCF for temperature extraction, respectively. 1 MHz frequency scanning step and 9 dB SNR are used for the measurement under different pump pulse widths. The temperature in the oven is set to be 50 °C.

respectively. Fig. 9(a) and (b) give the temperature uncertainty and RMSE measured under different SNRs with SVM-0.5 °C, LCF and pVCF for temperature extraction, respectively. The results are in agreement with the simulation depicted in Fig. 3 where at high SNR similar uncertainty and RMSE are observed for both SVM-0.5 °C and curve fitting methods, while at low SNR SVM-0.5 °C provides lower temperature uncertainty and RMSE than those of curve fitting methods. The results verify that SVM has good tolerance to SNR variation and can provide better accuracy when extracting temperature from noisy BGSs.

To analyze the performance of SVM for different spatial resolutions, we collect the BGSs by using different pump pulse widths (i.e., 80 ns, 40 ns, 30 ns, 25 ns, 20 ns, 15 ns). During the measurement, the frequency scanning step and SNR are fixed at 1 MHz and 9 dB, respectively. Fig. 10 shows temperature uncertainty and RMSE measured under different pump pulse width when using SVM-0.5 °C, LCF and pVCF for temperature extraction, respectively. We can see that at each pump pulse width, SVM-0.5 °C provides lower uncertainty and RMSE over the two

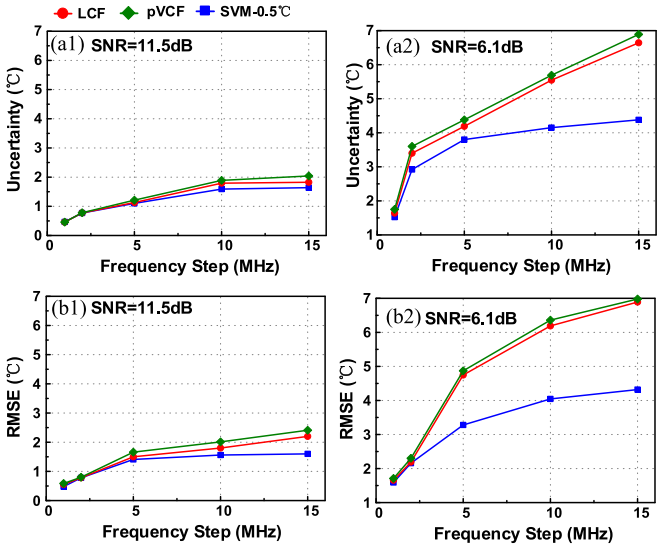


Fig. 11. (a1) & (a2) Temperature uncertainty, (b1) & (b2) RMSE measured by using SVM-0.5 °C, LCF and pVCF under 1000 and 50 times averaging, respectively. 20 ns pump pulse is used for the measurement under different frequency scanning steps. The temperature in the oven is set to be 50 °C.

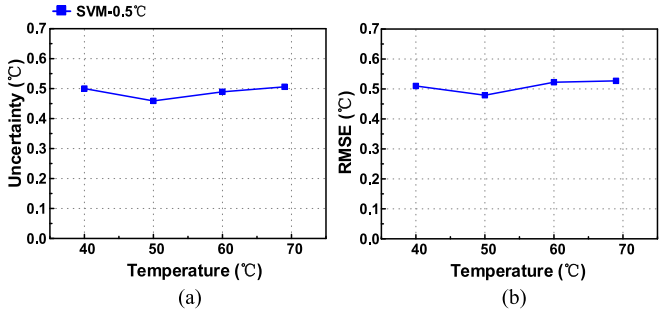


Fig. 12. (a) Temperature uncertainty, (b) RMSE measured by using SVM-0.5 °C when the temperature in the oven is set at 40 °C, 50 °C, 60 °C and 69 °C, respectively. 20 ns pump pulse, 1000 times averaging and 1 MHz scanning step are used for the measurement under different temperatures.

TABLE I
COMPARISON OF PROCESSING TIME USING SVM, LCF AND PVCF

| Frequency step | SVM-0.5℃ | | LCF | pVCF |
|---|---|---|---|---|
| | Training | Testing | | |
| 1MHz | 1.178 s | 15.75 s | 32.70 min | 36.12min |
| 2MHz | 0.916 s | 11.14 s | 23.19 min | 25.62min |
| 5MHz | 0.568 s | 11.06 s | 22.50 min | 24.75min |
| 10MHz | 0.451 s | 11.32 s | 22.19 min | 24.40min |
| 15MHz | 0.335 s | 12.55 s | 21.89 min | 24.08min |

curve fitting methods. For both SVM-0.5 °C and curve fitting methods, narrow pump pulse width gives rise to poor accuracy especially when the pulse width is smaller than 20 ns, e.g., at 15 ns pulse width, the temperature uncertainty and RMSE determined by SVM-0.5 °C are 1.137 °C and 1.22 °C, while they are 1.428 °C and 1.668 °C for LCF, 1.415 °C and 1.62 °C for pVCF, respectively. However, the degradation of uncertainty and RMSE using SVM-0.5 °C at narrow pulse width is less than that using LCF and pVCF, which matches well with the simulation in Fig. 4 and confirms that SVM has better tolerance to variations of pump pulse width than curve fitting methods. Therefore, only one SVM-0.5 °C model is enough to process the BGSs measured at different spatial resolutions.

The accuracy of temperature extraction also depends on the frequency scanning step used in the acquisition of BGSs. Fig. 11(a) shows the measured uncertainty under different frequency scanning steps, while Fig. 11(b) gives the RMSE versus frequency scanning step by using SVM-0.5 °C, LCF and pVCF, respectively. The BGSs are measured using 20 ns pump pulse with two different averaging times of 1000 and 50, corresponding to measured SNRs of 11.5 dB and 6.1 dB. Five frequency scanning steps, i.e., 1 MHz, 2 MHz, 5 MHz, 10 MHz, 15 MHz, corresponding to different data acquisition speed are employed. As the frequency step increases, fewer data points on each BGS are collected, resulting in the degradation of uncertainty and RMSE for both SVM-0.5 °C and curve fitting methods. At each frequency scanning step, temperature extraction using SVM-0.5 °C has lower uncertainty and RMSE compared with that using the two curve fitting methods, and the performance using SVM-0.5 °C degrades more slowly at large scanning step, especially when small averaging times i.e., low SNR is adopted, as depicted in Fig. 11(a2) and (b2). The results again are in agreement with the simulation in Fig. (5), implying better tolerance of SVM to different frequency scanning steps or acquisition speed, especially at low SNR.

The performance of SVM-0.5 °C under other temperatures is also evaluated. As the oven (Memmert UN10) we use can only be tuned at a minimum temperature step of 0.5 °C, we select four temperatures (40 °C, 50 °C, 60 °C and 69 °C) for the demonstration. Fig. 12(a) and (b) show the uncertainty and RMSE by using SVM-0.5 °C when the oven is set to 40 °C, 50 °C, 60 °C and 69 °C, respectively. The measurement is performed using pulse width of 20 ns, averaging times of 1000 and frequency scanning step of 1 MHz. Only little fluctuation under different temperatures is observed for both uncertainty and RMSE, which implies that SVM-0.5 °C can maintain good accuracy at a wide temperature range.

The data processing time used to extract temperature from the measured BGSs is an important parameter to evaluate the processing speed. Unlike ANN which requires time-consuming training phase to optimize multiple parameters (e.g., the number of layers, number of neurons in each layer and connecting weights among neurons), SVM possesses ultrafast training speed and requires less memory to store the model. Table I gives the time needed for the training of SVM-0.5 °C at different frequency scanning steps. The algorithms are implemented by using Matlab with i7-5960X CPU and 32G RAMs, and the number of training samples for SVM-0.5 °C are 21,816 according to Section II. The maximum training time is only 1.178 second, which is negligible when compared with several hours of ANN training time in Ref. [20]. Note that only 2806 training samples is used in Ref. [20] and much more time will be expected to train ANN using the same number of training samples as used here. Table I also shows the processing time using SVM-0.5 °C to extract temperature in the testing phase where

101,500 BGSs measured along 40.6 km FUT are processed (20 ns pump pulse width, 1000 averaging times and 250 MSample/s sampling rate). The processing time using LCF and pVCF for the same data set are also recorded for comparison. We can see that to process the collected BGSs at 1 MHz frequency scanning step, 32.7 minutes are needed using LCF and 36.12 minutes are needed for pVCF, but only 15.75 seconds are consumed using SVM-0.5 °C. The order of processing time using SVM-0.5 °C in the testing phase is at the level of 10 seconds and while that using LCF and pVCF are at least 20 minutes. The training and testing phases using SVM are completely independent, but even if the SVM training time is included in the data processing time, the processing speed using SVM-0.5 °C is still 100-fold faster than that using LCF and pVCF. Thus SVM can significantly reduce the processing time especially when a large number of sensing points are resolved and a number of BGSs are to be processed.

## IV. Conclusion

SVM has been successfully employed to process the BGSs and predict temperature information along the FUT in a BOTDA system. The BGSs serving as feature vectors are classified into each temperature class by the SVM models trained using ideal pseudo-Voigt curves with varying BFSs, linewidths and shape factors. Both simulation and experiment under different parameters for BGS collection are conducted to evaluate the performance of SVM. Three SVM models (SVM-1 °C, SVM-0.5 °C and SVM-0.1 °C) are established and found to provide almost the same performance in temperature extraction. At high SNR the temperature accuracy by SVM is comparable with that by the two curve fitting methods (i.e., LCF and pVCF), while at low SNR the performance of SVM is superior over LCF and pVCF, implying SVM has good tolerance to SNR variation and would be promising for long-distance sensing where SNR significantly degrades and noisy BGSs are usually collected. For different pump pulse widths, SVM provides lower uncertainty and RMSE over LCF and pVCF and the performance degradation using SVM at narrow pulse width is less than that using curve fitting methods, indicating SVM has better tolerance to variation of pump pulse width. The results also show that the performance of SVM at large scanning step degrades more slowly compared with that of LCF and pVCF, especially at low SNR, which means SVM can well accommodate a wide range of frequency scanning steps or acquisition speed.

More importantly, data processing speed using SVM to extract temperature information from the measured BGSs is very fast. Only less than 1.178s is needed in the training of SVM-0.5 °C with 21,816 training samples, and less than 15.75s is consumed to process 101,500 BGSs measured along 40.6 km FUT at 250 MSample/s sampling rate. The processing speed using SVM-0.5 °C is 100 times faster than that using LCF and pVCF even if the training time is included in the data processing time. It is especially useful where the number of resolved sensing points is large and fast measurement speed is required.

Compared with conventional curve fitting technique, the performance using SVM for temperature extraction is enhanced not only on the accuracy but also on the data processing speed, which would enable high-performance real-time BOTDA sensors in the future.

## References


[1] A. Kobyakov, M. Sauer, and D. Chowdhury, "Stimulated brillouin scattering in optical fibers," *Adv. Opt. Photon.*, vol. 2, no. 1, pp. 1–59, 2010.

[2] T. Horiguchi, K. Shimizu, T. Kurashima, M. Tateda, and Y. Koyamada, "Development of a distributed sensing technique using Brillouin scattering," *J. Lightw. Technol.*, vol. 13, no. 7, pp. 1296–1302, Jul. 1995.

[3] C. A. Galindez-Jamioy and J. M. Lopez-Higuera, "Brillouin distributed fiber sensors: An overview and applications," *J. Sens.*, vol. 2012, 2012, Art. no. 204121.

[4] X. Bao and L. Chen, "Recent progress in distributed fiber optic sensors," *Sensors*, vol. 12, no. 7, pp. 8601–8639, 2012.

[5] L. Thévenaz, "Brillouin distributed time-domain sensing in optical fibers: State of the art and perspectives," *Front. Optoelectron.*, vol. 3, no. 1, pp. 13–21, 2010.

[6] A. Motil, A. Bergman, and M. Tur, "State of the art of Brillouin fiber-optic distributed sensing," *Opt. Laser Technol.*, vol. 78, pp. 81–103, 2016.

[7] A. Barrias, J. R. Casas, and S. Villalba, "A review of distributed optical fiber sensors for civil engineering applications," *Sensors*, vol. 16, no. 5, p. 748, 2016.

[8] H. Cheng-Yu, Z. Yi-Fan, and L. Guo-Wei, "Recent progress of using Brillouin distributed fiber sensors for geotechnical health monitoring," *Sens. Actuators A, Phys.*, vol. 258, pp. 131–145, 2017.

[9] A. Masoudi and T. P. Newson, "Contributed Review: Distributed optical fibre dynamic strain sensing," *Rev. Sci. Instrum.*, vol. 87, 2016, Art. no. 011501.

[10] J. Dhliwayo, D. J. Webb, and C. N. Pannell, "Statistical analysis of temperature measurement errors in a Brillouin scattering-based distributed temperature sensor," *Proc. Int. Soc. Opt. Eng.*, vol. 2838, pp. 276–286, 1996.

[11] M. Niklès, L. Thévenaz, and P. A. Robert, "Brillouin gain spectrum characterization in single-mode optical fibers," *J. Lightw. Technol.*, vol. 15, no. 10, pp. 1842–1851, Oct. 1997.

[12] C. Li and Y. Li, "Fitting of Brillouin spectrum based on LabVIEW," in *Proc. 5th Int. Conf. Wirel. Commun., Netw. Mobile Comput.*, 2009, pp. 1–4.

[13] W. Zou, Z. He, and K. Hotate, "Complete discrimination of starin and temperature using Brillouin frequency shift and birefringence in a polarization-maintaining fiber," *Opt. Exp.*, vol. 17, no. 3, pp. 1248–1255, 2009.

[14] X. Bao, A. Brown, M. DeMerchant, and J. Smith, "Characterization of the Brillouin-loss spectrum of single-mode fibers by use of very short (<10-ns) pulses," *Opt. Lett.*, vol. 24, no. 8, pp. 510–512, 1999.

[15] G. A. Ferrier, S. Afshar, X. Bao, and L. Chen, "A new fitting method for spectral characterization of Brillouin-based distributed sensors," *Appl. Photon. Technol.*, vol. 5260, pp. 512–515, 2003.

[16] C. Zhang, Y. Yang, and A. Li, "Application of Levenberg–Marquardt algorithm in the Brillouin spectrum fitting," *Proc. SPIE*, vol. 7129, 2008, Art. no. 71291Y.

[17] M. A. Soto and L. Thévenaz, "Modeling and evaluating the performance of Brillouin distributed optical fiber sensors," *Opt. Exp.*, vol. 21, no. 25, pp. 31347–31366, 2013.

[18] M. A. Farahani, E. Castillo-Guerra, and B. G. Colpitts, "Accurate estimation of Brillouin frequency shift in Brillouin optical time domain analysis sensors using cross correlation," *Opt. Lett.*, vol. 36, no. 21, pp. 4275–4277, 2011.

[19] M. A. Farahani, E. Castillo-Guerra, and B. G. Colpitts, "A detailed evaluation of the correlation-based method used for estimation of the brillouin frequency shift in BOTDA sensors," *IEEE Sensors J.*, vol. 13, no. 12, pp. 4589–4598, Dec. 2013.

[20] A. K. Azad, L. Wang, N. Guo, H. Y. Tam, and C. Lu, "Signal processing using artificial neural network for BOTDA sensor system," *Opt. Exp.*, vol. 24, no. 6, pp. 6769–6782, 2016.

[21] C. J. Burges, "A tutorial on support vector machines for pattern recognition," *Data Mining Knowl. Disc.*, vol. 2, no. 2, pp. 121–167, 1998.

[22] V. Vapnik, *The Nature of Statistical Learning Theory*. New York, NY, USA: Springer Science & Business Media, 2013.

[23] C. L. Liu, K. Nakashima, H. Sako, and H. Fujisawa, "Handwritten digit recognition: benchmarking of state-of-the-art techniques," *Pattern Recog.*, vol. 36, no. 10, pp. 2271–2285, 2003.

[24] I. Guyon, J. Weston, S. Barnhill, and V. Vapnik, "Gene selection for cancer classification using support vector machines," *Mach. Learn.*, vol. 46, nos. 1–3, pp. 389–422, 2002.
[25] G. Mountrakis, J. Im, and C. Ogole, "Support vector machines in remote sensing: A review," *ISPRS J. Photogramm. Remote Sens.*, vol. 66, no. 3, pp. 247–259, 2011.
[26] E. Giacoumidis *et al.*, "Comparison of DSP-based nonlinear equalizers for intra-channel nonlinearity compensation in coherent optical OFDM," *Opt. Lett.*, vol. 41, no. 11, pp. 2509–2512, 2016.
[27] C. Cortes and V. Vapnik, "Support-vector networks," *Mach. Learn.*, vol. 20, no. 3, pp. 273–297, 1995.
[28] L. Bottou and C. J. Lin, "Support vector machine solvers," in *Large Scale Kernel Machines*. Cambridge, MA, USA: MIT Press, 2007, pp. 301–320.
[29] C. W. Hsu and C. J. Lin, "A comparison of methods for multiclass support vector machines," *IEEE Trans. Neural Netw.*, vol. 13, no. 2, pp. 415–425, Mar. 2002.
[30] A. Lopez-Gil *et al.*, "Evaluation of the accuracy of BOTDA systems based on the phase spectral response," *Opt. Exp.*, vol. 24, no. 15, pp. 17200–17214, 2016.
[31] M. A. Soto, J. A. Ramírez, and L. Thévenaz, "Intensifying the response of distributed optical fibre sensors using 2D and 3D image restoration," *Nature Commun.*, vol. 7, 2016, Art. no. 10870.

**Huan Wu** is currently working toward the Ph.D. degree in the Department of Electronic Engineering, The Chinese University of Hong Kong, Shatin, Hong Kong.

**Liang Wang** received the B.S. degree from Huazhong University of Science and Technology, Wuhan, China, in 2008, and the Ph.D. degree from The Chinese University of Hong Kong (CUHK), Shatin, Hong Kong, in 2013. From September 2013 to January 2014, he was a Research Scientist (core staff) with the Institute for Infocomm Research, A*STAR, Singapore. In February 2014, he joined the Photonics Research Center, The Hong Kong Polytechnic University, as a Postdoctoral Fellow, where was been awarded The Hong Kong Polytechnic University Postdoctoral Fellowships. Since September 2016, he has been an Assistant Professor (Research) in the Department of Electronic Engineering, CUHK. He has published more than 70 research papers in major peer-reviewed journals and international conferences. His research interests include fiber sensors, optical signal processing for optical communications, novel fiber devices, and photonic devices, etc.

**Nan Guo** is currently working toward the Ph.D. degree in the Department of Electronic and Information Engineering, HongKong Polytechnic University, Hong Kong.

**Chester Shu** (M'91–SM'02) received the Ph.D. degree in applied physics in 1991 from Columbia University, New York, NY, USA, where he performed graduate research on ultrafast optoelectronics.

He is currently a Professor in the Department of Electronic Engineering and the Center for Advanced Research in Photonics at the Chinese University of Hong Kong, Shatin, Hong Kong. He has contributed to nonlinear processing with specialty fibers and has developed unique approaches for polarization-insensitive parametric processing, processing of orthogonally polarized signals, bit-rate tunable, phase-sensitive, and wavelength-division optical processing. He has published more than 350 journals and conference papers and delivered a number of talks in the field. His research interests include optical signal processing for fiber communications and sensing.

Dr. Shu was a Topical Editor of *Optics Letters* in the area of fiber communications, from 2005 to 2011, and has served in a number of technical program committees including OFC/NFOEC, LEOS, and Photonics in Switching Conference. He was the Chairman of IEEE Hong Kong LEOS (currently Photonics Society) Chapter in 2006 and 2007.

**Chao Lu** obtained the B.Eng. degree in electronic engineering from Tsinghua University, Beijing, China, in 1985, and the M.Sc. and Ph.D. degrees from the University of Manchester, Manchester, U.K., in 1987 and 1990 respectively.

He joined the School of Electrical and Electronic Engineering, Nanyang Technological University (NTU), Singapore, in 1991 as a Lecturer and has served there as a Senior Lecturer and an Associate Professor until 2006. From June 2002 to December 2005, he was seconded to the Institute for Infocomm Research, Agency for Science, Technology and Research (A*STAR), Singapore, as the Program Director and Department Manager leading a research group in the area of optical communication and fiber devices. Since April 2006, he has been with the Department of Electronic and Information Engineering, The Hong Kong Polytechnic University, as a Professor. He was a Visiting Professor to the School of Electrical and Electronic Engineering, NTU, from Dec 2013 to Dec 2014. Over the years, he has published more than 220 papers in major international journals such as *Optics Express, Optics Letters*, IEEE PHOTONIC TECHNOLOGY LETTERS, and IEEE/OSA JOURNAL OF LIGHTWAVE TECHNOLOGY. He has presented many papers and has given a number of invited talks in major international conferences. He has been an organizer or technical program committee member of many international conferences. His research interests include optical communication systems and networks, fiber devices for optical communication, and sensor systems. In addition to academic research work, he has had many industrial collaborative research projects and has a number of awarded patents.

Dr. Lu is an Associate Editor of *Optics Express* and *Chinese Optics Letters*.